Electromechanical Properties of Ba$_{(1-x)}$Sr$_x$TiO$_3$ Perovskite Solid Solutions from First-Principles Calculations

Leonid L. Rusevich[1,2], Guntars Zvejnieks[1], Alessandro Erba[3], Roberto Dovesi[3],

and Eugene A. Kotomin[1*]

[1] Institute of Solid State Physics, University of Latvia, 8 Kengaraga str., Riga LV-1063, Latvia

[2] Institute of Physical Energetics, 11 Krivu str., Riga LV-1006, Latvia

[3] Dipartimento di Chimica, Università degli Studi di Torino, via Giuria 5, I-10125, Torino, Italy

Corresponding Author:

[*]E-mail: kotomin@latnet.lv   Phone: +371-67187480

Abstract

An enhancement of the piezoelectric properties of lead-free materials, which allow conversion of mechanical energy into electricity, is a task of great importance and interest. Results of first-principles calculations of piezoelectric/electromechanical properties of the $Ba_{(1-x)}Sr_xTiO_3$ (BSTO) ferroelectric solid solution with perovskite structure are presented and discussed. Calculations are performed within the linear combination of atomic orbitals (LCAO) approximation and periodic-boundary conditions, using advanced hybrid functionals of the density-functional-theory (DFT). A supercell model allows to investigate multiple chemical compositions x. In particular, three BSTO solid solutions with $x = 0, 0.125, 0.25$ are considered within the experimental stability domain of the ferroelectric tetragonal phase of the solid solution ($x<0.3$). The configurational disorder with $x=0.25$ composition is also investigated explicitly considering the seven possible atomic configurations corresponding to this composition. It is predicted that Sr-doping of $BaTiO_3$ makes it mechanically harder and enhances its electromechanical/piezoelectric properties which are important for relevant applications.

Introduction

In recent years, there has been an enormous interest in the efficient capture of environmental energy through the use of energy-harvesting devices that transform mechanical energy into electricity (refs 1 and 2 and references therein). In this respect, one of the most efficient ways is to utilize the piezoelectricity of nano-ferroelectrics.[3–5] In particular, ABO_3-type perovskite ferroelectrics are used for many technological applications and therefore have been intensively studied for a long time.[6–8] Lead-free $BaTiO_3$ (BTO) and $SrTiO_3$ (STO, an incipient ferroelectric) perovskites are among the most studied members of this class of materials.

The rapid progress of computational methods, on the one hand, and of the parallel performance of modern computer architectures, on the other hand, nowadays allow us to calculate the elastic and piezoelectric properties of perovskites based on a very accurate *ab initio* (first-principles) approach. Indeed, several calculations of piezoelectric properties of BTO crystals have recently been reported. In particular, Khalal *et al.*[9] and Meng *et al.*[10] studied elastic and piezoelectric properties of BTO in the tetragonal phase, whereas Mahmoud *et al.*[11] calculated piezoelectric, dielectric, elastic and photoelastic properties of BTO in its low-temperature rhombohedral phase.

From a structural point of view, both BTO and STO exhibit a cubic (paraelectric) phase at high temperature, where each Ti ion is octahedrally coordinated to six oxygen ions. This structure belongs to a centrosymmetric space group, *Pm-3m* (SG 221), and therefore cannot reveal ferro- and piezoelectricity, which are specific properties of non-centrosymmetric lattices. However, upon cooling, Ti ions are displaced along one of the cube main axes, which leads to a series of phase transitions. While STO undergoes a phase transition from the paraelectric cubic phase (SG 221) to another paraelectric tetragonal phase (*I4/mcm*, SG 140) at 105 K (ref 12), BTO undergoes

three consecutive ferroelectric transitions: at 393 K the crystalline symmetry reduces from cubic (SG 221) to tetragonal (*P4mm*, SG 99), then to orthorhombic (*Amm2*, SG 38) at 278 K and, lastly, to rhombohedral (*R3m*, SG 160) below 183 K (ref 11).

In this study, we focus our attention on the tetragonal (room temperature) ferroelectric BTO phase, which is the most interesting for technological applications.[6] An enhancement of the piezoelectric, ferroelectric and dielectric properties of perovskites can be achieved by engineering a lattice strain.[8,13] Partial replacement of atoms is one of the effective ways to produce lattice strain. Solid solutions near a morphotropic phase boundary, separating two crystal symmetries, are known to exhibit anomalously high piezoelectric and dielectric responses.[14] BTO is commonly doped by various impurity atoms, in order to improve its dielectric and electromechanical properties. In particular, a series of experimental papers was devoted to $Ba_{(1-x)}Sr_xTiO_3$ (BSTO) solid solutions with perovskite structure (refs 6, 7 and 15 and references therein) with a focus on dielectric properties. An artificial superlattice constructed from the two perovskites (e.g., BTO and STO) can also be applied to enhance piezoelectric and dielectric responses.[16,17]

The aim of this paper is the study of the electromechanical/piezoelectric properties of the tetragonal BSTO solid solution by means of first-principles calculations. The elastic and piezoelectric constants are computed, which show that the Sr-doping of BTO enhances its electromechanical properties. Advantage of $Ba_{(1-x)}Sr_xTiO_3$ solid solution, in contrast to BTO, is that the structural phase transition, which occurs in BTO at 5°C, shifts to lower temperatures at x increases.[18] As the result, there is no phase transition in BSTO in a wide temperature range around room temperature, what leads to a temperature-stable piezoelectric property, which is important for practical applications.

Computational Details

First-principles calculations are performed with the CRYSTAL14 code for quantum-chemical *ab initio* simulations,[19,20] which computes elastic and piezoelectric (direct and converse) tensors within a fully-automated procedure. The PBE0 hybrid DFT-HF exchange-correlation functional[21] is used, which already proved reliable for piezoelectric properties.[11,12] Hay and Wadt effective small core pseudopotentials[22–24] are used for Ba, Ti and Sr atoms, with $5s^2$, $5p^6$, $6s^2$ valence electrons for Ba; $3s^2$, $3p^6$, $3d^2$, $4s^2$ for Ti and $4s^2$, $4p^6$, $5s^2$ for Sr. The oxygen atoms are described by an all-electron basis set. The basis sets for Ba, Sr and Ti are taken from ref 25, where these were optimized for BTO and STO crystals, while the basis set for oxygen is taken from ref 26. All basis sets are available on the CRYSTAL website.[27]

In order to define an optimal set up for the calculations on the BSTO solid solution, we started from the calculation of the lattice constants, electronic properties, elastic and piezoelectric constants for several phases of BTO and STO crystals, and compared our results with both available experimental data and previous results of *ab initio* calculations (see below). Additionally, we performed calculations of lattice constants, band gap, bulk modulus, elastic and piezoelectric constants for the tetragonal BTO phase. Calculations have been performed with three hybrid functionals (see ref 20). The first one is the PBE0 functional, which combines PBE exchange functional with 25% of Hartree-Fock (HF) exchange and the PBE correlation functional. In the second, the exchange part in the PBE0 functional was replaced by the WCGGA (Wu-Cohen) exchange functional[28] with the same HF fractions (25%). This functional is designated in this paper as WC functional. Lastly, the third functional — B1WC combines the WCGGA exchange functional with 16% HF and the PWGGA (Perdew-Wang) correlation functional.

Our computational set up has been calibrated in terms of accuracy and computational time. In particular, the five thresholds governing the truncation of infinite lattice sums in the two-electron integral evaluation have been set to 8, 8, 8, 8, 16, and a regular Monkorst-Pack mesh of points in reciprocal space has been used, whose shrinking factor has been set to 12 and 6 for bulk and supercell calculations, respectively. These parameters ensure converged results.

A structural model for the BSTO solid solution has been built, which consists of a 2×2×2 supercell of the tetragonal BTO primitive unit cell. Such the supercell consists of 8 primitive BTO unit cells and, hence, it contains 40 atoms. In the supercell calculations, we have studied $Ba_{(1-x)}Sr_xTiO_3$ solutions with different compositions (i.e. Sr/Ba ratio), where Ba atoms are progressively replaced by Sr atoms. Thus, the calculations are performed for artificial ordered BSTO superstructures. We have performed calculations for three different Sr concentrations: without substitution (x=0.0; SC0); 1 Ba atom is replaced with 1 Sr atom (x=0.125; SC1); 2 Ba atoms are replaced with 2 Sr atoms (x=0.25; SC2). For the x=0.125 composition, any of the 8 Ba atoms in the cell could be substituted with a Sr atom. We replaced the Ba atom at the origin of the coordinate system — atom with coordinates *(0,0,0)* — to preserve as much symmetry as possible. For the x=0.25 composition, 2 Ba atoms are replaced with 2 Sr atoms: the one at the origin and a second one. All 7 possible configurations are here considered.

Results and Discussion

Before investigating the mechanical and piezoelectric response of BSTO solid solutions, we have calculated the elastic tensors for all the 4 phases of BTO, the piezoelectric (direct and converse) tensors for the 3 ferroelectric phases of BTO, and the elastic constants for cubic STO. Structural and elastic properties as well as the band gaps of the cubic phases of BTO and STO are given in

Table 1, where they are also compared with existing experimental data and with previous theoretical investigations performed with the same PBE0 functional. The cubic crystal system exhibits the simplest form of the symmetric elastic tensor, with only three independent constants (C_{11}, C_{12}, C_{44}). The agreement of our calculated values with previous theoretical investigations is remarkable, which confirms the accuracy of our computational setup. As expected, when comparing the calculated values for the elastic constants of these two high-temperature cubic phases with the experimental counterparts, they are found to be systematically larger, because thermal expansion was neglected in the calculations at this stage. Calculations for both cubic phases, BTO and STO, give indirect band gaps (Table 1). While for BTO the difference between indirect and direct values of band gap is very small (~30 meV), for STO this discrepancy is calculated significantly larger (~0.3 eV). The experimental difference in the direct and indirect band gap energies for a cubic STO is 0.5 eV (ref 35), slightly larger than calculated value. The absolute values of the calculated band gap energies are larger by ~25% than the experimental ones, which is much better than typical underestimate known for GGA-type functionals.[25]

The results of our BTO calculations in *tetragonal* phase are given in Table 2 (structural properties and band gap) and Table 3 (elastic and piezoelectric constants), along with available experimental values. As one can see, the PBE0 functional gives better agreement with experimental data for *a=b* lattice constant, while the WC and B1WC functionals — for *c* constant and tetragonal ratio *c/a*.

The computations of the BTO in the tetragonal phase predict an indirect band gap, which is very close for PBE0 and WC functionals, 4.08 eV (cf. 4.1 eV in ref 29 and 4.2 eV in ref 11), both larger than the experimental values[31] (see Table 2). On the other hand, the band gap, calculated by means of the B1WC functional, is very close to experimental data. The same is true for the cubic phase of BTO and STO — the B1WC band gap is closer to the experiments than that for

the PBE0 functional. Thus, the B1WC functional is well suited for the band gap calculations. Note also that the band gap likely depends more on the correlation part of functional rather than on the exchange one. Note that the calculations for tetragonal STO phase (SG 140) confirm the results of previous[41] hybrid calculations on the *direct* nature of the band gap as lowest in energy (unlike the STO cubic phase). The PBE0 calculations show that the band gap increases by 11 meV in the STO tetragonal phase as compared to the cubic phase (cf. 12 meV in ref 41).

The elastic tensor for the tetragonal phase of BTO (SG 99) has 6 independent constants, whereas direct and converse piezoelectric tensors only 3 independent components. The elastic and piezoelectric constants can be theoretically given as sums of purely electronic "clamped-ion" and nuclear (atomic) relaxation contributions. The results of the calculations for both the electronic contribution ("Clamped") and the total values ("Total"), including nuclear relaxation, are presented separately in Table 3. Almost for all elastic constants (except for C_{12}) the electronic contribution is larger than the total one, since the nuclear relaxation contributions for the elastic constants are negative. If the atoms are not allowed to relax ("clamped-ion" case), imposing of deformation shows more rigid material compared to the opposite case when atoms relax and thus the internal stress is reduced. As the result, we obtained larger elastic constants for the electronic term.

From Table 3 it is clearly seen that the origin of the piezoelectricity in BTO arises from the nuclear relaxation whereas the electronic "clamped-ion" contribution is rather small.

The calculated PBE0 bulk modulus for BTO in the tetragonal phase is 113 GPa. Previously calculated values (with the same functional) are 117 GPa (ref 11) and 112 GPa (ref 29). For both cubic and tetragonal phases we obtained a good agreement with previous theoretical results and experimental data for the lattice constants and elastic properties. A rather large discrepancy is however observed between calculated and experimental values of the piezoelectric constants.

Note, however, a broad dispersion of relevant experimental data. Therefore, we focus mainly on the trends in electromechanical property changes rather than in absolute values. The results of our calculations show that the PBE0 functional provides a slightly better description of piezoelectric properties, and, further, in tables we present only the results of PBE0 calculations.

The calculated Mulliken atomic charges for BTO in cubic and tetragonal phases are presented in Table 4. Our computed charges coincide with those in ref 29, calculated for the cubic phase. These charges indicate a considerable covalent contribution to the Ti-O chemical bonds, and small variation in charges of non-equivalent O ions in the tetragonal phase.

As mentioned above, to model the BSTO solid solution, we used 40 atom supercells. Any of the 8 Ba atoms in such supercells could be replaced by Sr atoms. When no Ba atoms are substituted, the x=0 chemical composition is called SC0. When only one Ba atom is replaced (SC1), the Sr atom is put at the origin of the coordinates, to maximize the residual point-symmetry. When two Ba atoms are replaced (SC2), the first Sr is placed at the origin and the second Sr replaces one of the 7 remaining Ba atoms. By default, we consider the second atom with fractional coordinates *(0.5,0.5,0.5)* in the supercell. We discuss below the effect of configurational disorder.

The results of our calculations for the elastic and piezoelectric properties of the BSTO solid solution for $x = 0$, 0.125 and 0.25 are reported in Table 5, where they are compared with those of the BTO tetragonal bulk crystal (with 5 atoms in the unit cell). First of all, we notice that all elastic and most of piezoelectric constants of the x=0 case (SC0) coincide with those computed for the bulk BTO phase. However, this is not the case for the piezoelectric constants $e_{15}=e_{24}$ and $d_{15}=d_{24}$, which show a large discrepancy. Unlike these two calculations which are expected to provide exactly the same results for a low-temperature stable phase, this is not guaranteed when a *high-temperature* phase is studied at 0 K (as performed in the standard DFT calculations).

Indeed, in this case, a mechanical lattice instability occurs (related to presence of the vibrational modes with imaginary frequencies in the **k**-point other than the Γ in the phonon Brillouin zone) when the fourth strain component (according to Voigt's notation) is applied to the lattice, which is a shear strain involving lattice angle deformations and a drastic symmetry reduction (from 8 to 2 operations). This analysis is confirmed by purely electronic "clamped-ion" calculations without nuclear relaxation, which provide the same piezoelectric constants both for the unit cell (bulk) and the supercell (SC0) calculations.

Let us now analyze the effect of an increased concentration of Sr-doping on the elastic and piezoelectric properties of the BSTO solid solution as a function of concentration x (Table 5). The main elastic constants of the system increase as a function of Sr concentration, which makes the system more rigid. Interestingly, a clear systematic (almost linear) increase of the piezoelectric response is also observed. Indeed, the absolute values of all piezoelectric constants increase with the Sr content. An enhancement of the piezoelectric response by 13÷30% is documented for the x=0.25 composition. The considerable effect of the substitution of Ba with Sr atoms on the electronic polarization properties is also observed in the atomic charges. The Mulliken atomic charges of Sr atoms are $1.88\,e$, compared to $1.80\,e$ for Ba atoms in the unperturbed BTO, which corresponds to a more ionic bonding. At the same time, the atomic charges of Ba and Ti atoms in the solid solution are practically unchanged.

We studied the limited Sr concentration range of x=0÷0.25 because, as known from experimental data,[18,42,43] at room temperature and around x≈0.3 the BSTO solid solution undergoes the ferroelectric to paraelectric transition, from the tetragonal to cubic phase. For higher Sr concentrations, the solid solution thus exhibits a cubic symmetry without piezoelectric properties.

When studying the solid solution, one has to take into account the configurational disorder of the system. For a given structural model (here, a supercell containing 40 atoms), many independent structural configurations could exist for a given chemical composition. For the x=0.25 composition, two of the eight Ba atoms are substituted with Sr atoms. The first Ba atom, which was replaced by Sr atom, was located at the origin of the coordinates. In Table 6 we report selected structural, elastic and piezoelectric features of the 7 possible configurations obtained by substituting, one at a time, the other 7 Ba atoms by Sr. Our supercell contains 2 pairs of symmetry-related Ba atoms: *(0.5,0,0.5)–(0,0.5,0.5)* (marked with an asterisk in Table 6) and *(0.5,0,0)–(0,0.5,0)* (marked with two asterisks). If one of them is replaced with a Sr atom, the equivalence is lost in both pairs and the symmetry of the system reduces from tetragonal down to orthorhombic. For example, when atoms *(0,0,0)* and *(0.5,0.5,0.5)* are replaced, the symmetry is still tetragonal, which implies that $a=b\neq c$ and that there are equivalent elements in the elastic and piezoelectric tensors, but when atoms *(0,0,0)* and *(0.5,0,0.5)* are replaced, the symmetry becomes orthorhombic with $a\neq b\neq c$ and without equivalence among elastic and piezoelectric constants.

The results, reported in Table 6, clearly demonstrates that in this case the configurational disorder is only marginally affecting the average properties of the solid solution. The elastic constants are almost independent of the particular selected configuration with differences among configurations less than 4%. Most piezoelectric coefficients also show a little dispersion as the function of different atomic configurations. Here it is necessary to mention that the differences of the electronic energies for these configurations are so small (<0.09 eV) that no reliable conclusion could be drawn about relative configuration stabilities. More detailed analysis based on the Gibbs free energies would be necessary which is beyond the scope of the present study.

Note in conclusion that it was predicted[44] for the ordered BSTO structure that it is thermodynamically unstable with respect to the heterophase mixture BTO and STO, i.e. spinodal

decomposition of the solid solution should occur (ordered solid solutions were discussed in refs 45 and 46). As a consequence, at relative small concentration of Sr, clusters of STO could arise in a predominantly BTO matrix. However, this process could be very slow due to very slow diffusion rate of cations in solid solution, especially at room temperature.

Conclusions

We performed the first theoretical study of the electromechanical/piezoelectric properties of the tetragonal (room temperature) $Ba_{(1-x)}Sr_xTiO_3$ solid solution by means of first-principles calculations based on advanced hybrid functionals of the density-functional-theory. The supercell model was used for calculation of electromechanical properties of perovskite solid solutions. Three compositions ($x=0$, $x=0.125$ and $x=0.25$) have been considered within the range where the solid solution is experimentally known to exhibit a ferroelectric behavior.

The present calculations clearly predict that the $BaTiO_3$ perovskite becomes mechanically harder when Ba atoms are progressively substituted with Sr atoms. Interestingly, a significant and almost linear enhancement of the piezoelectric properties of $BaTiO_3$ is predicted upon substitution of Ba with Sr atoms. Indeed, the e_{33} direct piezoelectric coefficient is found to increase by ~30% for $x=0.25$. Our calculations revealed that the nuclear relaxation rather than the electronic term contributes mainly to the BTO and BSTO piezoelectricity. On the other hand, the configurational disorder marginally affects the computed mechanical and piezoelectric properties of the BSTO solid solution. The study of other dopants, e.g. Ca, would be of interest.

Acknowledgements

References

(1)   Pruvost, S.; Hajjaji, A.; Lebrun, L.; Guyomar, D.; Boughaleb, Y. Domain Switching and Energy Harvesting Capabilities in Ferroelectric Materials. *J. Phys. Chem. C* **2010**, *114*, 20629–20635.

(2)   Bowen, C. R.; Kim, H. A.; Weaver, P. M.; Dunn, S. Piezoelectric and Ferroelectric Materials and Structures for Energy Harvesting Applications. *Energy Environ. Sci.* **2014**, *7*, 25–44.

(3)   Park, K.; Xu, S.; Liu, Y.; Hwang, G.; Kang, S. L.; Wang, Z. L.; Lee, K. J. Piezoelectric BaTiO$_3$ Thin Film Nanogenerator on Plastic Substrates. *Nano Lett*. **2010**, *10*, 4939–4943.

(4)   Yan, J.; Jeong, Y. G. High Performance Flexible Piezoelectric Nanogenerators Based on BaTiO$_3$ Nanofibers in Different Alignment Modes. *ACS Appl. Mater. Interfaces* **2016**, *8*, 15700–15709.

(5)   Sevik, C.; Çakir, D.; Gülseren, O.; Peeters, F. M. Peculiar Piezoelectric Properties of Soft Two-Dimensional Materials. *J. Phys. Chem. C* **2016**, *120*, 13948–13953.

(6)   Lines, M. E.; Glass, A. M. *Principles and Applications of Ferroelectrics and Related Materials*; Clarendon: Oxford, 1977.

(7)   Smolensky, G. A.; Bokov, V. A.; Isupov, V. A.; Krainik, N. N.; Pasynkov, R. E.; Sokolov, A. I.; Yushin, N. K. *Ferroelectrics and Related Materials*; Gordon and Breach: New York, 1984.

(8)   Damjanovic, D. Ferroelectric, Dielectric and Piezoelectric Properties of Ferroelectric Thin Films and Ceramics. *Rep. Prog. Phys.* **1998**, *61*, 1267–1324.

(9)   Khalal, A.; Khatib, D.; Jannot, B. Elastic and Piezoelectric Properties of BaTiO$_3$ at Room Temperature. *Physica B* **1999**, *271*, 343–347.

(10) Meng, X.; Wen, X.; Qin, G. DFT Study on Elastic and Piezoelectric Properties of Tetragonal BaTiO$_3$. *Comput. Mater. Sci.*, **2010**, *49*, S372–S377.

(11) Mahmoud, A.; Erba, A.; El-Kelany, Kh. E.; Rerat, M.; Orlando, R. Low-Temperature Phase of BaTiO$_3$: Piezoelectric, Dielectric, Elastic, and Photoelastic Properties from *Ab Initio* Simulations. *Phys. Rev. B* **2014**, *89*, 045103.

(12) Erba, A.; El-Kelany, Kh. E.; Ferrero, M.; Baraille, I.; Rerat, M. Piezoelectricity of SrTiO$_3$: An *Ab Initio* Description. *Phys. Rev. B* **2013**, *88*, 035102.

(13) Haeni, J. H.; Irvin, P.; Chang, W.; Uecker, R.; Reiche, P.; Li, Y. L.; Choudhury, S.; Tian, W.; Hawley, M. E.; Craigo B., et al. Room-Temperature Ferroelectricity in Strained SrTiO$_3$. *Nature* **2004**, *430*, 758–761.

(14) Gao, J.; Hu, X.; Liu, Y.; Wang, Y.; Ke, X.; Wang, D.; Zhong, L.; Ren, X. Ferroelectric Domain Walls Approaching Morphotropic Phase Boundary. *J. Phys. Chem. C* **2017**, *121*, 2243–2250.

(15) Jaffe, B.; Cook, W. R.; Jaffe, H. *Piezoelectric Ceramics*; Academic: New York, 1971.

(16) Lebedev, A. I. *Ab Initio* Studies of Dielectric, Piezoelectric, and Elastic Properties of BaTiO$_3$/SrTiO$_3$ Ferroelectric Superlattices. *Phys. Solid State* **2009**, *51*, 2324–2333.

(17) Hu, D.; Ma, H.; Tanaka, Y.; Zhao, L.; Feng, Q. Ferroelectric Mesocrystalline BaTiO$_3$/SrTiO$_3$ Nanocomposites with Enhanced Dielectric and Piezoelectric Responses. *Chem. Mater.* **2015**, *27*, 4983–4994.

(18) Lemanov, V. V.; Smirnova, E. P.; Syrnikov, P. P.; Tarakanov, E. A. Phase Transitions and Glasslike Behavior in Sr$_{1-x}$Ba$_x$TiO$_3$. *Phys. Rev. B* **1996**, *54*, 3151–3157.

(19) Dovesi, R.; Orlando, R.; Erba, A.; Zicovich-Wilson, C. M.; Civalleri, B.; Casassa, S.; Maschio, L.; Ferrabone, M.; De La Pierre, M.; D'Arco, P., et al. CRYSTAL14: A Program

for the *Ab Initio* Investigation of Crystalline Solids. *Int. J. Quantum Chem.* **2014**, *114*, 1287–1317.

(20) Dovesi, R.; Saunders, V. R.; Roetti, C.; Orlando, R.; Zicovich-Wilson, C. M.; Pascale, F.; Civalleri, B.; Doll, K.; Harrison, N. M.; Bush, I. J., et al. *CRYSTAL14 User's Manual*; University of Torino: Torino, 2014.

(21) Adamo, C.; Barone, V. Toward Reliable Density Functional Methods without Adjustable Parameters: The PBE0 Model. *J. Chem. Phys.* **1999**, *110*, 6158–6170.

(22) Hay, P. J.; Wadt, W. R. *Ab Initio* Effective Core Potentials for Molecular Calculations. Potentials for the Transition Metal Atoms Sc to Hg. *J. Chem. Phys.* **1985**, *82*, 270–283.

(23) Wadt, W. R.; Hay, P. J. *Ab Initio* Effective Core Potentials for Molecular Calculations. Potentials for Main Group Elements Na to Bi. *J. Chem. Phys.* **1985**, *82*, 284–298.

(24) Hay, P. J.; Wadt, W. R. *Ab Initio* Effective Core Potentials for Molecular Calculations. Potentials for K to Au Including the Outermost Core Orbitals. *J. Chem. Phys.* **1985**, *82*, 299–310.

(25) Piskunov, S.; Heifets, E.; Eglitis, R. I.; Borstel, G. Bulk Properties and Electronic Structure of $SrTiO_3$, $BaTiO_3$, $PbTiO_3$ Perovskites: an *Ab Initio* HF/DFT Study. *Comput. Mater. Sci.* **2004**, *29*, 165–178.

(26) Bredow, T.; Jug, K.; Evarestov, R. A. Electronic and Magnetic Structure of $ScMnO_3$. *Phys. Stat. Sol. (b)* **2006**, *243*, R10–R12.

(27) CRYSTAL — Basis Sets Library. http://www.crystal.unito.it/basis-sets.php, (accessed November 15, 2017).

(28) Wu, Z.; Cohen, R. E. More Accurate Generalized Gradient Approximation for Solids. *Phys. Rev. B* **2006**, *73*, 235116.

(29) Evarestov, R. A.; Bandura, A. V. First-Principles Calculations on the Four Phases of BaTiO$_3$. *J. Comput. Chem.* **2012**, *33*, 1123–1130.

(30) *Ternary Compounds, Organic Semiconductors*; Madelung, O., Rössler, U., Schulz M., Eds.; Springer Berlin Heidelberg: Berlin, 2000; Vol. 41E of the series Landolt-Börnstein – Group III Condensed Matter.

(31) Wemple, S. H. Polarization Fluctuations and the Optical-Absorption Edge in BaTiO$_3$. *Phys. Rev. B* **1970**, *2*, 2679–2689.

(32) Wang, J. J.; Meng, F. Y.; Ma, X. Q.; Xu, M. X.; Chen, L. Q. Lattice, Elastic, Polarization, and Electrostrictive Properties of BaTiO$_3$ from First-Principles. *J. Appl. Phys.* **2010**, *108*, 034107.

(33) Evarestov, R. A.; Blokhin, E.; Gryaznov, D.; Kotomin, E. A.; Maier, J. Phonon Calculations in Cubic and Tetragonal Phases of SrTiO$_3$: A Comparative LCAO and Plane-Wave Study. *Phys. Rev. B* **2011**, *83*, 134108.

(34) Cao, L.; Sozontov, E.; Zegenhagen, J. Cubic to Tetragonal Phase Transition of SrTiO$_3$ under Epitaxial Stress: An X-Ray Backscattering Study. *Phys. Stat. Sol. (a)* **2000**, *181*, 387–404.

(35) van Benthem, K.; Elsässer, C.; French, R. H. Bulk Electronic Structure of SrTiO$_3$: Experiment and Theory. *J. Appl. Phys.* **2001**, *90*, 6156–6164.

(36) Bell, R. O.; Rupprecht, G. Elastic Constants of Strontium Titanate. *Phys. Rev.* **1963**, *129*, 90–94.

(37) Fischer, G. J.; Wang, Z.; Karato, S. Elasticity of CaTiO$_3$, SrTiO$_3$ and BaTiO$_3$ Perovskites up to 3.0 GPa: the Effect of Crystallographic Structure. *Phys. Chem. Minerals* **1993**, *20*, 97–103.

(38) Zgonik, M.; Bernasconi, P.; Duelli, M.; Schlesser, R.; Günter, P.; Garrett, M. H.; Rytz, D.; Zhu, Y.; Wu, X. Dielectric, Elastic, Piezoelectric, Electro-Optic, and Elasto-Optic Tensors of $BaTiO_3$ Crystals. *Phys. Rev. B* **1994**, *50*, 5941–5949.

(39) Berlincourt, D.; Jaffe, H. Elastic and Piezoelectric Coefficients of Single-Crystal Barium Titanate. *Phys. Rev.* **1958**, *111*, 143–148.

(40) Davis, M.; Budimir, M.; Damjanovic, D.; Setter, N. Rotator and Extender Ferroelectrics: Importance of the Shear Coefficient to the Piezoelectric Properties of Domain-Engineered Crystals and Ceramics. *J. Appl. Phys.* **2007**, *101*, 054112.

(41) Heifets, E.; Kotomin, E.; Trepakov, V. A. Calculations for Antiferrodistortive Phase of $SrTiO_3$ Perovskite: Hybrid Density Functional Study. *J. Phys.: Condens. Matter.* **2006**, *18*, 4845–4851.

(42) Barb, D.; Barbulescu, E.; Barbulescu, A. Diffuse Phase Transitions and Ferroelectric-Paraelectric Diagram for the $BaTiO_3$-$SrTiO_3$ System. *Phys. Stat. Sol. (a)* **1982**, *74*, 79–83.

(43) Kim, S. W.; Choi, H. I.; Lee, M. H.; Park, J. S.; Kim, D. J.; Do, D.; Kim, M. H.; Song, T. K.; Kim, W. J. Electrical Properties and Phase of $BaTiO_3$-$SrTiO_3$ Solid Solution. *Ceramics International* **2013**, *39*, S487–S490.

(44) Fuks, D.; Dorfman, S.; Piskunov, S.; Kotomin, E. A. Ab Initio Thermodynamics of $Ba_cSr_{(1-c)}TiO_3$ Solid Solutions. *Phys. Rev. B* **2005**, *71*, 014111.

(45) Cohen, R. E.; Heifets, E.; Fu, H. First-Principles Computation of Elasticity of $Pb(Zr,Ti)O_3$: The Importance of Elasticity in Piezoelectrics. *AIP Conference Proceedings* **2001**, *582*, 11–22.

(46) Heifets, E.; Cohen, R. E. Ab initio Study of Elastic Properties of $Pb(Ti,Zr)O_3$. *AIP Conference Proceedings* **2002**, *626*, 150–159.

Tables

	This study	PBE0	Expt
BTO, SG 221			
a, Å	3.993	3.98 [11]; 3.99 [29]	3.996 [30]
E_g^*, eV	3.97	4.0 [11,29]	3.2 [31]
C_{11}, GPa	328.5		206 [25]; 255 [32]
C_{12}, GPa	120.5		140 [25]; 82 [32]
C_{44}, GPa	147.7		126 [25]; 108 [32]
B, GPa	189.8	194 [11]; 189 [29]	162 [11,29]; 195 [11]
STO, SG 221			
a, Å	3.901	3.91 [33]	3.905 [34]
E_g^{**}, eV	4.16 (4.47)	3.9 (4.2) [33]	3.25 (3.75) [35]
C_{11}, GPa	367.6	370 [12]	317.6 [36]
C_{12}, GPa	113.6	114 [12]	102.5 [36]
C_{44}, GPa	134.2	133 [12]	123.5 [36]
B, GPa	198.2	199 [12]; 195 [33]	179 [37]

[*] The experimental band gap energy[31] for BTO corresponds to temperature around 130°C, i.e. above the phase transition temperature.

[**] Indirect (direct) band gap.

PBE0 — earlier calculated data.

Table 1. Lattice Constant a, Band Gap E_g, Elastic Constants C_{ij} and Bulk Modulus B for the Cubic Structures of BTO and STO.

	PBE0	WC	B1WC	Expt
Lattice constants, Å				
$a=b$	3.971	3.950	3.962	3.992 [30]
c	4.131	4.032	4.050	4.036 [30]
c/a	1.040	1.021	1.022	1.011
Band gap, eV				
E_g*	4.08	4.07	3.26	3.38 (3.27) [31]

* Experimental values[31] at room temperature for light polarized parallel (and perpendicular) to the

ferroelectric *c* axis.

Data are calculated using PBE0, Wu-Cohen (WC) and B1WC functionals.

Table 2. Structural Properties and Band Gap of BTO for Tetragonal Phase (SG 99).

	PBE0		WC		B1WC		Expt[*]
	Total	Clamped	Total	Clamped	Total	Clamped	
Elastic constants, GPa							
$C_{11}=C_{22}$	302.7	314.1	337.5	346.1	325.1	333.4	222; 275
C_{12}	120.8	118.1	127.8	126.9	124.4	122.8	134; 179
$C_{13}=C_{23}$	88.4	115.0	98.0	123.2	96.1	118.7	111; 152
C_{33}	118.6	309.3	166.4	346.9	159.8	333.8	151; 165
$C_{44}=C_{55}$	89.8	129.3	116.6	142.1	110.4	135.5	61.1; 54.4
C_{66}	141.2	141.2	149.5	149.5	142.8	142.8	134; 113
B	112.6	181.5	143.3	198.4	138.7	191.2	134 [11]; 141 [11]
Direct piezoelectric constants, C/m^2							
$e_{15}=e_{24}$	10.116	0.199	9.205	0.148	9.354	0.152	34.2 [38]
$e_{31}=e_{32}$	0.686	0.274	0.804	0.230	0.763	0.233	-0.7 [38]
e_{33}	3.293	-0.471	4.357	-0.399	4.213	-0.403	6.7 [38]
Converse piezoelectric constants, pC/N=pm/V							
$d_{15}=d_{24}$	112.674	1.536	78.935	1.041	84.699	1.120	392 [39]; 564 [40]
$d_{31}=d_{32}$	-6.062	1.296	-5.038	0.964	-5.296	1.013	-34.5 [39]; -33.4 [40]
d_{33}	36.811	-2.485	32.126	-1.835	32.733	-1.928	85.6 [39]; 90 [40]

[*] Ref 32 and references there.

Data are calculated using PBE0, Wu-Cohen (WC) and B1WC functionals. Purely electronic ("Clamped") contribution and total values of constants ("Total"), including nuclear relaxation contribution, are presented.

Table 3. Bulk Modulus (B), Elastic and Piezoelectric Constants of BTO for Tetragonal Phase (SG 99).

	Ba	Ti	O1	O2	O3
SG 221	1.797	2.392	-1.396	-1.396	-1.396
SG 99	1.801	2.367	-1.361	-1.403	-1.403

Table 4. Mulliken Atomic Charge (*e*) for Cubic (SG 221) and Tetragonal (SG 99) BTO Phases.

	Bulk	SC0	SC1	SC2
Elastic constants, GPa				
$C_{11}=C_{22}$	302.7	302.6	307.3	311.5
C_{12}	120.8	120.8	120.4	120.2
$C_{13}=C_{23}$	88.4	88.5	89.3	90.5
C_{33}	118.6	118.3	123.5	130.3
$C_{44}=C_{55}$	89.8	89.8	92.6	95.8
C_{66}	141.2	141.2	133.4	137.3
B	112.6	112.5	116.1	120.7
Direct piezoelectric constants, C/m^2				
$e_{15}=e_{24}$	10.116	-2.101	-2.397	-2.717
$e_{31}=e_{32}$	0.686	0.679	0.740	0.839
e_{33}	3.293	3.294	3.719	4.270
Converse piezoelectric constants, pC/N=pm/V				
$d_{15}=d_{24}$	112.674	-23.381	-25.895	-28.350
$d_{31}=d_{32}$	-6.062	-6.124	-6.522	-6.947
d_{33}	36.811	36.987	39.546	42.404

"Bulk" — perfect crystal, SC0 — without substitution of atoms, SC1 — 1 Ba atom (at the coordinate origin) is replaced with Sr atom, SC2 — 2 Ba atoms (at the coordinate origin and with fractional coordinates *(0.5,0.5,0.5)*) are replaced with 2 Sr atoms. B — bulk modulus.
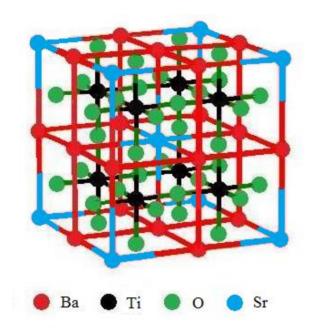
Table 5. Elastic and Piezoelectric Constants, Calculated for Perfect Bulk Crystal BTO (SG 99) and 3 Supercells.

	SC2 (replacement of 2 Ba atoms: with coordinates *(0,0,0)* and *another one*)						
	xyz	*xy0*	*0yz**	*x0z**	*0y0***	*x00***	*00z*
Lattice constants, Å							
a	7.909	7.913	7.907	7.910	7.9080	7.9079	7.910
b	$=a$	$=a$	7.910	7.907	7.9079	7.9080	$=a$
c	8.136	8.128	8.142	8.142	8.142	8.142	8.132
Elastic constants, GPa							
C_{11}	311.5	312.7	313.326	311.932	312.079	313.315	313.0
C_{12}	120.2	121.7	119.068	119.063	119.794	119.785	119.7
C_{13}	90.5	89.4	89.334	91.345	90.326	90.776	90.2
C_{22}	$=C_{11}$	$=C_{11}$	311.901	313.295	313.319	312.006	$=C_{11}$
C_{23}	$=C_{13}$	$=C_{13}$	91.266	89.299	90.876	90.220	$=C_{13}$
C_{33}	130.3	134.6	130.935	130.956	129.911	129.679	135.6
Direct piezoelectric constants, C/m^2							
e_{31}	0.839	0.802	0.811	0.836	0.793	0.759	0.817
e_{32}	$=e_{31}$	$=e_{31}$	0.838	0.812	0.755	0.798	$=e_{31}$
e_{33}	4.270	4.190	4.206	4.205	4.124	4.131	4.199
Converse piezoelectric constants, pC/N=pm/V							
d_{31}	-6.947	-6.278	-6.599	-6.943	-6.731	-7.009	-6.313
d_{32}	$=d_{31}$	$=d_{31}$	-6.923	-6.580	-7.002	-6.734	$=d_{31}$
d_{33}	42.404	39.469	41.451	41.439	41.323	41.444	39.356

Second Ba atoms, which are replaced with Sr atoms, are specified in the title of the columns (the first is atom at the coordinate origin). Designations of atoms: *xyz* — atom with fractional coordinates *(0.5,0.5,0.5)*, *xy0* — with coordinates *(0.5,0.5,0)* etc.

Table 6. Lattice Constants and Selected Elastic and Piezoelectric Constants of the BSTO Solid Solution for the *x*=0.25 Chemical Composition, as Calculated for All Possible Atomic Configurations.

TOC Graphic